Published in final edited form as:
Nat Photonics. 2008 ; 2(2): 110–115. doi:10.1038/nphoton.2007.297.

OPTICAL PHASE CONJUGATION FOR TURBIDITY SUPPRESSION IN BIOLOGICAL SAMPLES

Zahid Yaqoob[1], **Demetri Psaltis**[1,2], **Michael S. Feld**[3], and **Changhuei Yang**[1,*]

[1] Electrical Engineering, California Institute of Technology, 1200 E California Blvd., Pasadena, CA 91125, USA [2] School of Engineering, Ecole Polytechnique Federale de Lausanne, CH-1015 Lausanne, Switzerland [3] G. R. Harrison Spectroscopy Laboratory, Massachusetts Institute of Technology, 77 Massachusetts Avenue 6−207, Cambridge, MA 02139, USA

Abstract

Elastic optical scattering, the dominant light interaction process in biological tissues, prevents tissues from being transparent. While scattering may appear stochastic, it is in fact deterministic in nature. We show that, despite experimental imperfections, optical phase conjugation ($\lambda = 532$ nm) can force a transmitted light field to retrace its trajectory through a biological target and recover the original light field. For a 0.69 mm thick chicken breast tissue section, we can enhance point source light return by ~5×10^3 times and achieve a light transmission enhancement factor of 3.8 within a collection angle of 29°. Additionally, we find that the reconstruction's quality, measured by the width of the reconstructed point source, is independent of tissue thickness (up to 0.69 mm thick). This phenomenon may be used to enhance light transmission through tissue, enable measurement of small tissue movements, and form the basis of new tissue imaging techniques.

Elastic optical scattering in biological tissue typically dominates over absorption by an order of magnitude or more. As a point of reference, consider light propagation in chicken breast tissue at wavelength 633 nm; the scattering coefficient is 23 mm^{-1} and the reduced scattering coefficient is 0.8 mm^{-1}, whereas the mean absorption coefficient is only 0.01 mm^{-1} [1]. Being the dominant light interaction process, scattering prevents tissue from being transparent by distorting and effectively randomizing the transmission light field paths. Yet, it is also known that elastic optical scattering is a deterministic and time-reversible process. In other words, if we can record the phase and amplitude of the propagating scattered light field completely and reproduce a back propagating phase conjugated (or time-reversed) field, this field should be able to retrace its trajectory through the scattering medium and return the original input light field. In fact, more than 40 years ago, Leith et al. demonstrated that optical phase conjugation (OPC) could reverse optical scattering induced by a ground glass slide [2]. While OPC has been used in numerous laser-related applications such as high-resolution imaging 3, laser resonators 4, 5, and pulse compression [6], its use in suppressing turbidity in biomedical applications has remained largely unexplored. The use of interferometric wavefront sensing and holography techniques in biomedical optics has largely focused on phase imaging and the selection of minimally scattered light for imaging [7-9]. Finally, we note that there have been significant investigations of phase conjugation techniques in the microwave and ultrasound regimes. Their utility ranges from enhancing acoustic energy delivery to target brain tumors or kidney stones

*For correspondence and requests for material, contact Prof. Changhuei Yang (email: chyang@caltech.edu)..

COMPETING FINANCIAL INTERESTS: The authors declare no competing financial interests.

[10] to enabling sub-wavelength focusing of microwaves for increased information transfer rate per unit volume [11].

Most of these techniques have the potential to be translated into optical regime equivalents for biomedical applications if OPC can suppress scattering in biological tissues. To accomplish this, three challenges must be addressed: 1) As tissues are highly scattering, light propagating beyond a certain tissue thickness (> 100 μm in general) is predominantly multiply scattered. In our experiments, the mean number of scattering events per photon is as high as 26 for a 0.69 mm thick chicken breast tissue section. Previous optical experiments did not come close to this level of turbidity. It is an open question as to whether turbidity suppression in tissue via OPC is observable as the effect can be expected to be more prone to noise and sensitive to the reconstruction condition as scattering increases. 2) It is not feasible to record the entire scattered light field. There is a recording angle range associated with most forms of optical wavefront recording media such as holographic plates, photorefractive crystals, etc., beyond which the recording efficiency declines significantly. In addition, a fraction of the light field illuminating a sufficiently thick tissue section will be backscattered. As such, it is reasonable to question whether an incompletely phase conjugated light field can adequately retrace its trajectory in the biological target. 3) Some of the light will be absorbed by the tissue. This breaks the time direction symmetry associated with that light component.

This paper presents a first-of-its-kind study of optical phase conjugation for turbidity suppression in biological tissues, which we call “turbidity suppression by optical phase conjugation” (TSOPC). We show that while the above three factors can impact the quality and extent of the reconstruction, turbidity suppression can nevertheless be observed for sections of chicken breast tissue up to 0.69 mm thick at λ=532 nm. We also characterize the key features associated with this phenomenon.

RESULTS

Demonstration of TSOPC in Biological Tissues

The salient features of TSOPC are well illustrated in the first experiment. We employed a photorefractive 45°-cut 0.075% Fe-doped Lithium Niobate ($LiNbO_3$) crystal as the OPC light field generator or phase conjugate mirror (PCM); the recording-and-playback scheme [Fig. 1 (a)] is detailed in the Method section. In this study, our target was a 0.46 mm thick chicken breast tissue section. Light at 532 nm, 3.5 mW power and $1/e^2$ beam size of 0.7 mm was transmitted through a standard negative USAF resolution target. The patterned light was then imaged onto the front face (face 1) of the tissue section using a 1:1 imaging relay lens. The forward scattered light traversed the tissue sample, exited from face 2, and arrived at the photorefractive crystal for holographic recording. The recording geometry is highlighted in Fig. 1(b). In the experiment, the separation between the crystal facet and the tissue section was 0.5 mm. The 7.8 mm $1/e^2$ diameter 6.5 mW reference beam employed during the recording process crossed the crystal at 1 mm distance from the crystal facet facing the tissue section. This implies a nominal maximum recording angle range of 66°. The hologram recording time was ~2 minutes for this experiment. Upon completion, the USAF resolution target was replaced with a compensation glass plate and an OPC light field was generated with a conjugate reference beam of 12 mW. This light field retraced the path of the original transmission and recreated an image of the USAF target on face 1 of the tissue [Fig. 1(c)]. This image was then relayed onto a CCD camera (DMK 31BF03, The Imaging Source).

Mathematically [see Fig. 1(d)], the interaction of incident light field $\begin{pmatrix} \mathbf{a}_1 \\ \mathbf{a}_2 \end{pmatrix}$ with a scattering medium can be expressed as [12]:

$$\begin{pmatrix} \mathbf{b}_1 \\ \mathbf{b}_2 \end{pmatrix} = \begin{pmatrix} \bar{S}_{11} & \bar{S}_{12} \\ \bar{S}_{21} & \bar{S}_{22} \end{pmatrix} \begin{pmatrix} \mathbf{a}_1 \\ \mathbf{a}_2 \end{pmatrix}, \quad (1)$$

where $\begin{pmatrix} \bar{S}_{11} & \bar{S}_{12} \\ \bar{S}_{21} & \bar{S}_{22} \end{pmatrix}$ is the scattering matrix associated with the medium, $\begin{pmatrix} \mathbf{b}_1 \\ \mathbf{b}_2 \end{pmatrix}$ is the output light field and $\mathbf{a}_2 = 0$. The subscript denotes the terminal face 1 or 2 of the scattering medium. In this case, the light field impinging on the PCM is given by $\bar{S}_{21}\mathbf{a}_1$. The OPC light field traveling back towards face 2 of the tissue section can be expressed as:

$$\psi_{phase\quad conjugate} = \bar{A}\ \bar{S}_{21}{}^{*}\ \mathbf{a}_1^{*}, \quad (2)$$

where $\bar{A}$ represents the reduction in angular range of the reconstructed wave due to the incomplete recording and playback of the transmitted wave. The reconstructed light field on face 1 of the tissue section can be written as:

$$\psi_{reconstructed} = \bar{S}_{12}\ \bar{A}\ \bar{S}_{21}{}^{*}\ \mathbf{a}_1^{*}. \quad (3)$$

Since the relationship between any two points on the medium's surface is symmetrical we get $\bar{S}_{21} = \bar{S}_{12}{}^{T}$.

In an ideal case, 1) the capture of the initial light transmission is complete; this leads to a reduction of $\bar{A}$ to a unitary matrix, 2) medium is lossless and backscattering is absent; this leads to $\bar{S}_{12}\bar{S}_{12}{}^{\dagger} = \mathrm{I}$ by energy conservation, where $\bar{S}_{12}{}^{\dagger}$ is the complex conjugate of $\bar{S}_{12}{}^{T}$. The reconstructed light field expression can then be written as:

$$\psi_{ideal,reconstructed} = \bar{S}_{12}\bar{S}_{12}{}^{\dagger}\ \mathbf{a}_1^{*} = \mathbf{a}_1^{*}. \quad (4)$$

The extent to which an experimental realization approaches this ideal is verified in our experiment. Figure 2(c) shows the reconstructed USAF image through the 0.46 mm thick tissue section. For comparison, Figs. 2(a) and 2(b) show USAF target imaging through 0.46 mm thick agarose and tissue section, respectively, using plane wave illumination. At 532 nm, the chicken breast tissue scattering coefficient was 38 mm^{-1} (quantified through interferometric measurement of ballistically propagating transmission through tissue) and the sum of the reduced scattering coefficient and the absorption coefficient was 0.45 mm^{-1} (quantified through transmission measurement). This implies that, on average, a photon is scattered 17 times in a 0.46 mm thick tissue sample, and 19% of the input light did not reach face 2 of the 0.46 mm thick tissue section. The high quality of the reconstructed image in Fig. 2(c) demonstrates that the conjugated signal beam can indeed retrace its initial trajectory through the tissue to a good degree, in spite of these issues.

TSOPC Experiments using Point Source Illumination

The next set of experiments studied the TSOPC phenomenon in a more quantitative fashion. In this case, we focused 0.65 mW signal beam to a 1.4 μm $1/e^2$ diameter spot via L3 (Olympus PLAN 10×) at the face 1 of the tissue section [see Fig. 3(a)].

Each experiment consisted of the following. The transmitted light through the tissue section was first holographically recorded in the photorefractive crystal for 30 sec with a reference beam power of 33 mW. Next, a conjugate reference beam (3.3 mW) was used to generate the OPC light field, which traveled back through the tissue section and reconstructed the original light spot at face 1 of the tissue section. We displaced the tissue sample laterally in incremental steps to a limit of 8 μm and acquired an image of the reconstructed spot for each displacement. Four targets were employed – a 0.23 mm thick clear agarose section (non-scattering control) and chicken breast tissue sections of thickness 0.23 mm, 0.46 mm and 0.69 mm. The experiment was repeated 8 times for each sample thickness. For the agarose section, the average return power through the sample was measured as 0.4 nW. This value was a function of the readout reference beam power and the crystal's recording efficiency. To eliminate contributions of these two experimental parameters from our analysis, we normalized our data with respect to our measurements from the agarose control.

We found that, under these experimental conditions, the strength of a recorded hologram decreased minimally over the experimental time frame of ~2 minutes for each TSOPC experiment (see Supplementary Fig. 1) and, as such, does not impact on our findings significantly. We also note that the efficiency of the TSOPC reconstruction is expected to drop as the biological samples change in time, but experimentally, we did not observe a significant change over the time in which each experiment was conducted.

Figures 3(b)-(f) illustrate the average radial light intensity distribution in the reconstructed spot for 0 μm, 2 μm, 4 μm, 6 μm and 8 μm displacements, respectively, of the 0.23 mm thick agarose sample (magenta) and the tissue sections of thickness 0.23 mm (black), 0.46 mm (red), and 0.69 mm (blue). Two observations are noteworthy. First, while a significant tissue section displacement leads to a mismatch between the scattering structures and the returning OPC light field, and results in no turbidity suppression, it can be observed from Fig. 3(c) that this phenomenon is tolerant to small sample displacements, particularly for thinner samples. Second, Fig. 3(b) illustrates that the width of the fully reconstructed spot appears surprisingly similar for all tissue thickness.

Figure 4(a) shows normalized peak intensity as a function of sample lateral displacement. Several observations are worth noting: 1) The reconstructed peak intensity falls as a sample is displaced. This is predictable, as displacements of the sample disrupt the light trajectory retracing condition and deteriorate the reconstruction. 2) The extent to which the reconstructed peak appeared to be reconstructed is remarkable. For the 0.69 mm thick tissue section, the reconstructed peak intensity difference between zero sample displacement (optimal reconstruction condition) and large sample displacement of 8 μm (mismatched sample and OPC light field) is more than 3 orders of magnitude. 3) The rate of reconstructed peak intensity drop due to sample lateral translation is a function of the sample thickness; for a 0.69 mm thick chicken tissue section, a displacement of ~0.7 μm results in peak intensity reduction by one order of magnitude. 4) Finally, the reconstruction appears surprisingly robust. With our thickest tissue section of 0.69 mm, the reconstructed peak intensity was still a respectable (17 ± 3) % of the agarose reconstructed peak intensity.

The dependence of specific reconstruction efficiency on tissue thickness can be seen from Fig. 4(b). We plotted the relative reconstructed peak intensity on the same scale for zero sample displacement. We can realistically expect the loss of scattering information from light being absorbed by the tissue and/or scattered away from the crystal to deteriorate the reconstruction. Simplistically, we can conjecture that the reconstructed peak height with no sample displacement will follow a Beer's Law-type dependency on tissue thickness for thin tissue sections. In other words, the reconstructed peak intensity I_{peak} is proportional to $\exp(-\alpha L)$, where α is the coefficient associated with the drop in reconstruction efficiency and L is the

thickness of the tissue section. Fig. 4(b) reveals that such a dependency does indeed hold well for the thin tissue sections (~0.46 mm or less), for which an experimental fit for α is (1.45 ± 0.05) mm^{-1}. For thicker tissues, the drop-off in reconstruction efficiency appears to deviate from this trend. The exact behavior of the reconstruction efficiency is an important subject that deserves further in depth study. For comparison, we have added a line in Fig. 4(b) that shows the unscattered light attenuation as a function of tissue depth; this line shows an expected signal drop associated with coherence based interference detection methods. We can see from Fig. 4 (b) that the rate of TSOPC efficiency drop occurs at a much slower rate, which clearly indicates that the TSOPC phenomenon is able to make good use of multiply scattered light components.

Figure 4(c) shows the change in normalized transmission collected through the objective as a function of sample lateral displacement. This parameter is different from the reconstructed peak intensity in that it tracks the total amount of light that is returned from the sample (and falls within the collection angle, 29°, of the objective) even if the reconstruction is imperfect. The data trace for the 0.69 mm thick section is particularly revealing. Comparing the normalized transmission between when TSOPC is present (zero sample displacement) and absent (~2.5 μm sample displacement), we can see that TSOPC pushes the total light transmission up by a factor of 3.8. This clearly indicates that TSOPC can be used to achieve enhanced light transmission through biological tissues.

Figure 5(a) plots the $1/e^2$ width of the reconstructed spot as a function of sample displacement. Under optimal reconstruction condition (zero sample displacement), the reconstructed spot is tight for all the sample thicknesses, as also shown in Figs. 3(b) and 5(b). However, as the displacement increases, the $1/e^2$ spot size widens. The results in Fig. 5(a) also indicate that the rate of $1/e^2$ width increase with sample displacement is a function of sample thickness or scattering extent. Further, we can see from the plots in Fig 5(a) as well as Figs. 3(b)-(f), the reconstructed light spot appeared to consist of two components – a sharp well-reconstructed spot and a more diffused spot. The more diffused spot grew in strength as the sample was displaced and likely consisted of light components that were weakly reconstructed. In comparison, the well-reconstructed spot dropped in intensity with sample displacement but did not appear to increase in width significantly.

More intriguingly, Fig. 5(b) revealed that the $1/e^2$ width for all tissue thicknesses at zero tissue displacement is approximately the same (1.5 μm). This is in good agreement with the estimated $1/e^2$ spot size of 1.4 μm for perfect reconstruction. The insensitivity to tissue thickness and the good fit to the theoretically predicted width for ideal reconstruction suggest that there exists a phase conjugate component that can retrace the initial light trajectory optimally even if the phase conjugation process as a whole is necessarily imperfect due to experimental constraints.

DISCUSSION

There are numerous ways to generate OPC light field, including static holography [13, 14], stimulated scattering [15, 16], real-time holography [17, 18], four-wave mixing [19, 20], and six-wave mixing [21]. One can also conceivably combine a wavefront sensor, such as a digital holography system (see Supplementary Fig. 2) or a Shack-Hartman array, with a spatial light modulator to create an electronically controllable PCM. Our experiments employed a static holography approach, as this allowed us to defer the OPC light field playback – a feature needed for the sample-OPC light field mismatch experiment.

Dynamic OPC light field generation methods, such as four-wave mixing [19, 20] or an electronically controllable PCM, are particularly promising as the means for implementing TSOPC based applications. As there is no appreciable time delay between light field recording and playback in these methods, the effect of minute movements of cellular components and

fluid tissues in living tissue, which can disrupt the reconstruction condition, is effectively nullified. On the other hand, the sensitivity of static holography-based OPC schemes to minute movements can be adapted to enable high sensitivity movement measurements. In addition, we note that while the crystal chosen for these experiments erases itself with time and light exposure, there exist permanent holographic recording media, such as self-developing photopolymer-based recording media [22].

The applications of TSOPC are potentially wide ranging. For example, it may potentially be used to enhance light delivery for therapeutic purposes such as photodynamic therapy, in a manner analogous to the use of ultrasound-based time-reversal phenomenon to deliver high ultrasound dosages for kidney stones [10] removal. TSOPC's ability to enhance light transmission can potentially be used to improve the depth penetration of imaging methods, such as photoacoustic tomography [23, 24].

To summarize, we have demonstrated tissue turbidity suppression with optical phase conjugation. In our experiments, the mean number of scattering events can reach up to 26 for the 0.69 mm thick chicken tissue. Further, a significant fraction of the light field never reached the photorefractive crystal in our experiment (27% of the light is backscattered by the 0.69 mm thick chicken tissue section). In spite of issues with tissue absorption and incomplete optical wavefront recording/readout, this newly observed biophotonics phenomenon has proved to be remarkably robust.

Our experiments demonstrate that it is possible to reconstruct a point source deteriorated by passage through 0.69 mm thick tissue such that it is more than 3 orders of magnitude above the background. In addition, the amount of tolerable tissue and OPC field mismatch is relatively large (~0.7 μm for an order of magnitude reconstruction drop for 0.69 mm thick chicken breast tissue section). This is a relevant practical consideration for certain applications. Our experiments also indicate that for zero displacement of the tissue sections, the phenomenon roughly obeys a Beer's Law-type dependence on tissue thickness [attenuation coefficient = $(1.45 \pm 0.05)\ \mathrm{mm}^{-1}$] for thin tissue sections. In addition, we found that the quality of the reconstruction (as measured by the width of an optimal reconstructed peak) is independent of tissue thickness for thicknesses up to 0.69 mm; this point is surprising as one would reasonably expect a deterioration in reconstruction quality as well. Finally, we can enhance overall tissue transmission with TSOPC; we observed an increase in transmission by a factor of 3.8 compared to non-TSOPC transmission for 0.69 mm thick tissue within a collection angle of 29°.

METHOD

The experimental setup for generating the OPC light field is shown in Fig. 1(a). Light from a 532 nm DPSS laser (Coherent Inc.) was spatially filtered and collimated ($1/e^2$ beam diameter 7.8 mm). This beam then passed through a half wave plate (WP1) and was split into two by a polarization beam splitter (P1). The reflected (vertically-polarized) and the transmitted (horizontally-polarized) beams formed the sample arm and reference arms, respectively. Another half wave plate (WP2), oriented at 45°, changed the polarization state of the reference beam to vertical, causing it to reflect from the second polarization beam splitter (P2) and reach the photorefractive crystal. The combined reference and signal beams then created a holographic pattern in the photorefractive crystal.

To generate the OPC light field, the half wave plate WP2 was rotated so that the wave plate direction was coincident with the polarization of the incoming reference beam. The outgoing light remained horizontally polarized, passed straight through the polarization beam splitter P2, and reached the photorefractive crystal via mirrors M2, M3 and M4 for reading out the stored hologram. A half wave plate (WP3) oriented at 45°, placed in the path of the read beam,

and changed its polarization back to vertical. The position and orientation of each mirror was adjusted so that the read beam was not only coincident with the recording beam but counter-propagating, as well. In this geometry, an OPC light field was generated which retraced the path of original light field and was detected by means of a CCD via lenses L4 and L5 in Fig. 1(a). The reconstruction process of the conjugate signal beam using a conjugate reference beam is shown schematically in Fig. 1(c).

Acknowledgments

This work was supported by NSF career award BES-0547657 and DARPA Center for Optofluidic Integration.

REFERENCES

1. Cheong WF, Prahl SA, Welch AJ. A review of the optical-properties of biological tissues. IEEE J. Quantum Electron 1990;26:2166–2185.
2. Leith EN, Upatneiks J. Holographic imagery through diffusing media. J. Opt. Soc. Am 1966;56:523.
3. Levenson MD. High-resolution imaging by wave-front conjugation. Opt. Lett 1980;5:182–184. [PubMed: 19693165]
4. McFarlane RA, Steel DG. Laser-oscillator using resonator with self-pumped phase-conjugate mirror. Opt. Lett 1983;8:208–210. [PubMed: 19714186]
5. Gower MC. Krf laser-amplifier with phase-conjugate Brillouin retro-reflectors. Opt. Lett 1982;7:423–425. [PubMed: 19714043]
6. Tomov IV, Fedosejevs R, McKen DCD, Domier C, Offenberger AA. Phase conjugation and pulse-compression of Krf-laser radiation by stimulated Raman-scattering. Opt. Lett 1983;8:9–11. [PubMed: 19714118]
7. Leith E, et al. Imaging through Scattering Media with Holography. J. Opt. Soc. Am. A - Opt. Image Science Vision 1992;9:1148–1153.
8. Jones R, et al. Holographic storage and high background imaging using photorefractive multiple quantum wells. Appl. Phys. Lett 1996;69:1837–1839.
9. Cuche E, Bevilacqua F, Depeursinge C. Digital holography for quantitative phase-contrast imaging. Opt. Lett 1999;24:291–293. [PubMed: 18071483]
10. Fink M. Time-reversed acoustics. Sci. Am 1999;281:91–97.
11. Lerosey G, De Rosny J, Tourin A, Fink M. Focusing beyond the diffraction limit with far-field time reversal. Science 2007;315:1120–1122. [PubMed: 17322059]
12. Mittra R, Habashy TM. Theory of wave-front-distortion correction by phase conjugation. J. Opt. Soc. Am. A -Opt. Image Science Vision 1984;1:1103–1109.
13. Gabor D. A new microscopic principle. Nature 1948;161:777–778. [PubMed: 18860291]
14. Lukosz W. Equivalent-lens theory of holographic imaging. J. Opt. Soc. Am 1968;58:1084–&.
15. Zel'dovich BY, Popovich VI, Ragul'skii VV, Faizullov FS. Connection between wave fronts of reflected and exciting light in stimulated Mandelshtam-Brillouin scattering. JETP Lett.-USSR 1972;15:109–113.
16. Hellwarth RW. Theory of phase conjugation by stimulated scattering in a waveguide. J. Opt. Soc. Am 1978;68:1050–1056.
17. Ivakin EV, Petrovich IP, Rubanov AS, Stepanov BI. Dynamic holograms in amplifying medium. Kvantovaya Elektronika 1975;2:1556–1558.
18. Gunter P. Holography, Coherent-light amplification and optical-phase conjugation with photorefractive materials. Phys. Rep.-Rev. Sec. Phys. Lett 1982;93:199–299.
19. Yariv A. Phase conjugate optics and real-time holography. IEEE J. Quantum Electron 1978;14:650–660.
20. Hellwarth RW. Generation of time-reversed wave fronts by nonlinear refraction. J. Opt. Soc. Am 1977;67:1–3.
21. Charra F, Nunzi JM. Nondegenerate multiwave mixing in polydiacetylene - Phase Conjugation with Frequency-Conversion. J. Opt. Soc. Am. B - Opt. Phys 1991;8:570–577.

22. Cheben P, Calvo ML. A photopolymerizable glass with diffraction efficiency near 100% for holographic storage. Appl. Phys. Lett 2001;78:1490–1492.

23. Hoelen CGA, de Mul FFM, Pongers R, Dekker A. Three-dimensional photoacoustic imaging of blood vessels in tissue. Opt. Lett 1998;23:648–650. [PubMed: 18084605]

24. Wang XD, et al. Noninvasive laser-induced photoacoustic tomography for structural and functional in vivo imaging of the brain. Nature Biotech 2003;21:803–806.

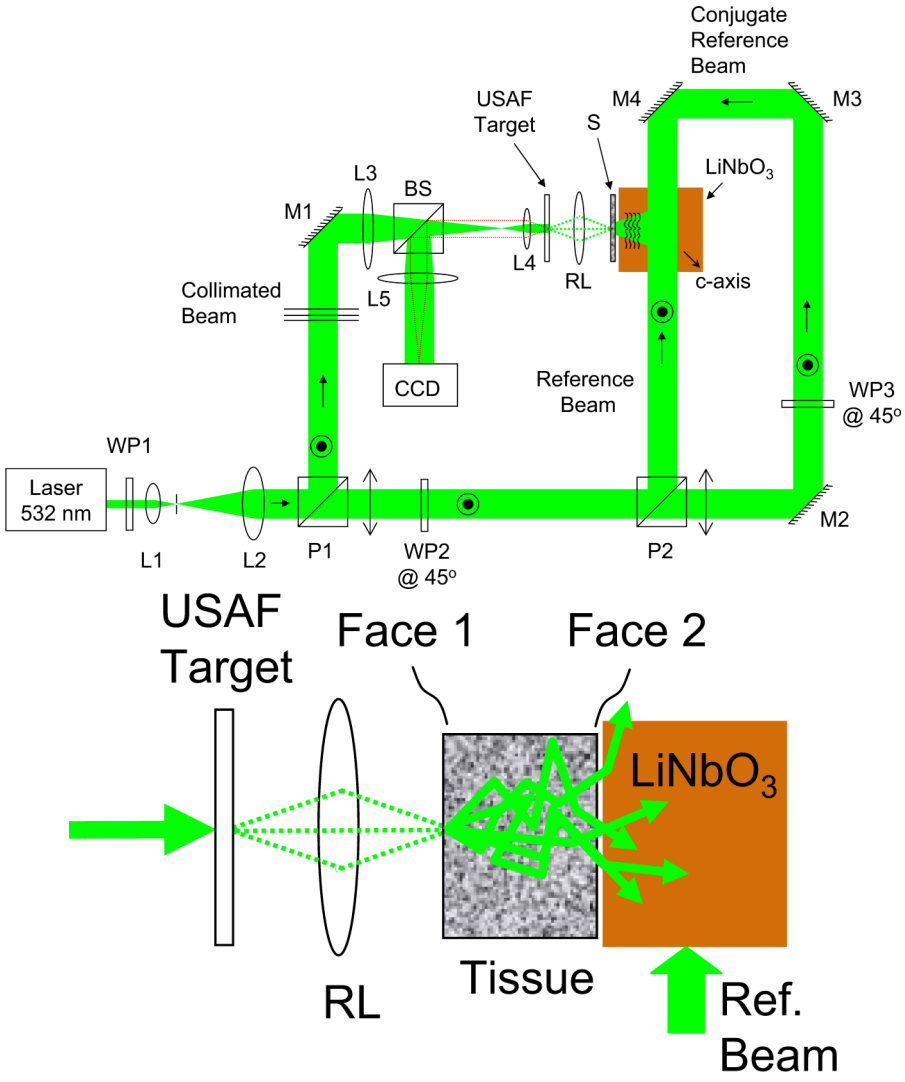

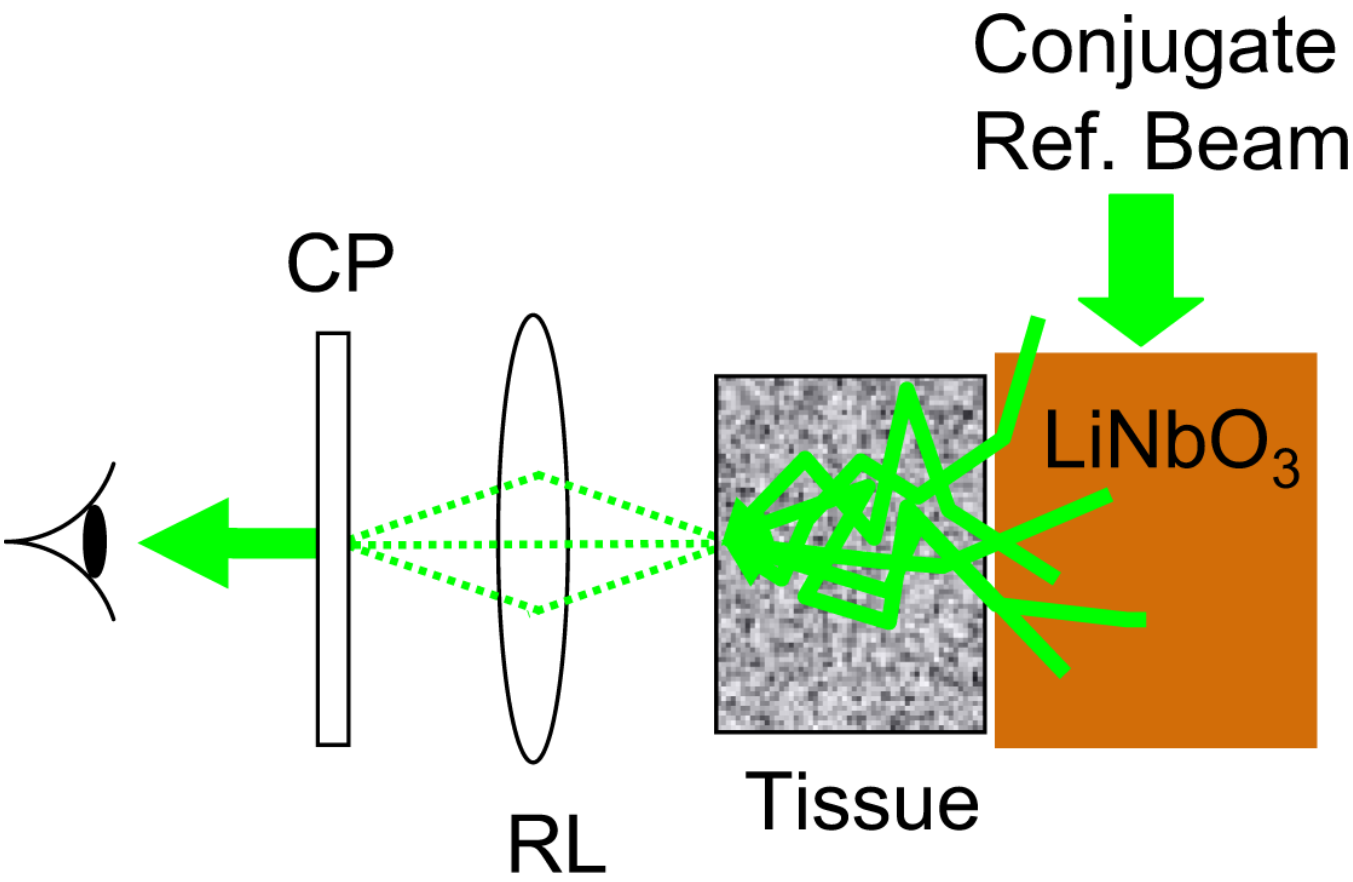

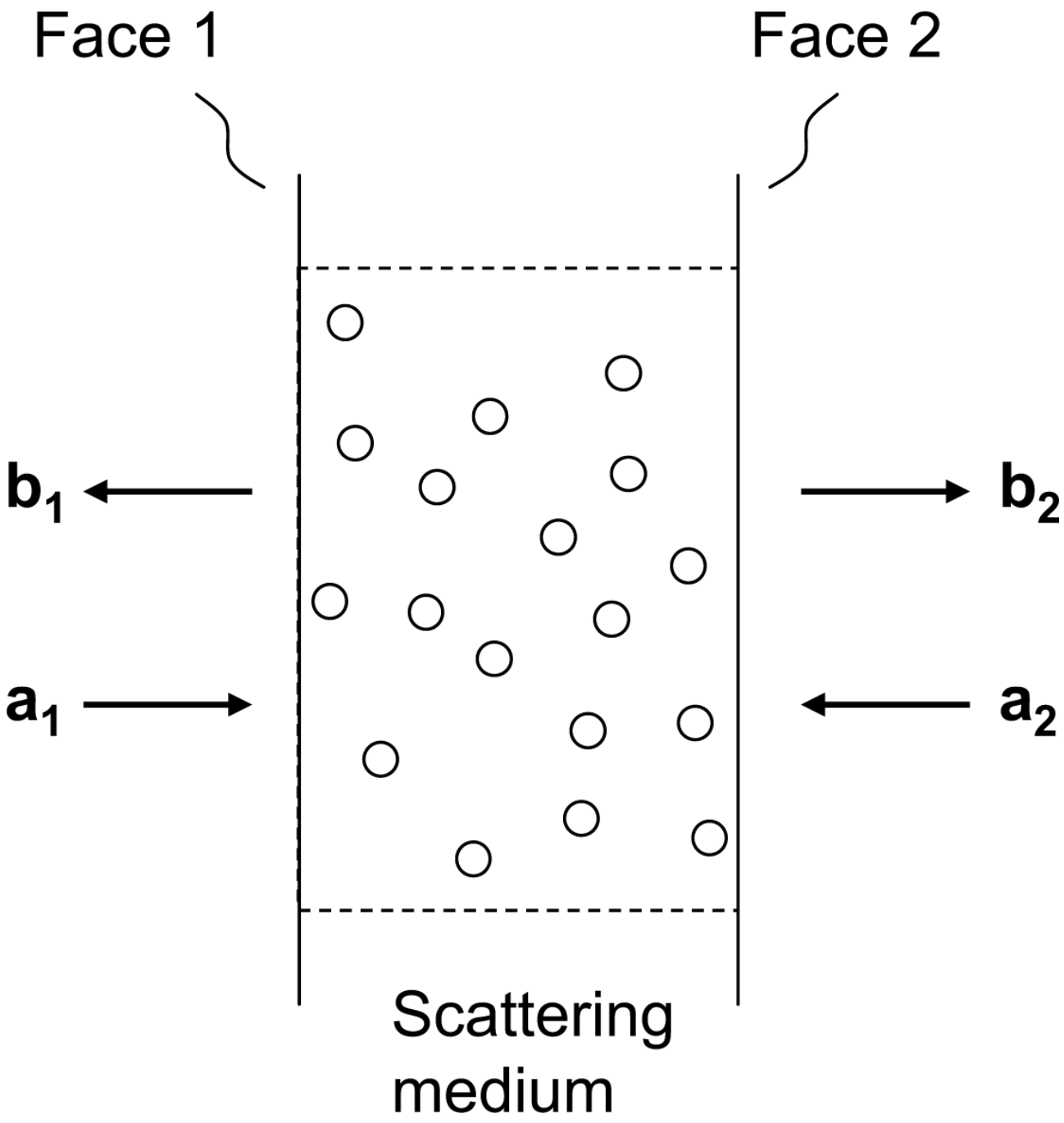

Figure 1. Schematics of TSOPC setup and scattering medium

(a) Experimental setup to confirm the TSOPC phenomenon in biological tissues. Concentric (black) dot and circle represent vertical polarization whereas double arrow in the plane of paper symbolizes horizontal polarization. (b) and (c) show schematics for recording of tissue turbidity information and reconstruction of OPC light field, respectively. (d) Schematic of a scattering medium. $\mathbf{a_i}$ and $\mathbf{b_i}$ are the complex incident and scattered fields, respectively, at the i^{th} face of the scattering medium. Li; ith spherical lens; RL: relay lens; CP: compensation plate; Mi: ith mirror; WPi: ith half wave plate; Pi: ith polarization beam splitter; BS: 50/50 beam splitter; CCD: charge coupled device; S: scattering sample.

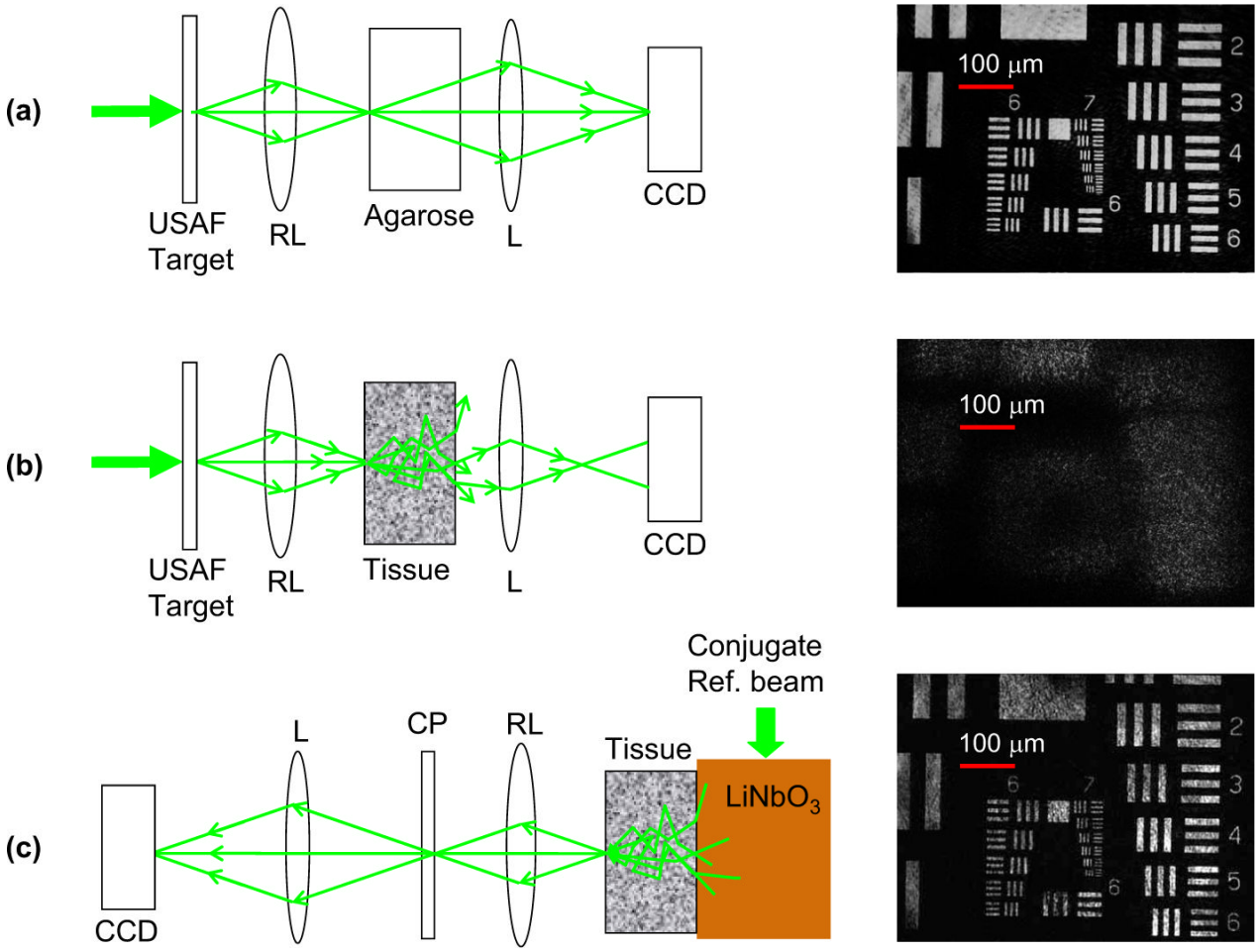

Figure 2. Demonstration of the TSOPC phenomenon through 0.46 mm thick chicken breast tissue section

(a,b) show imaging of USAF target through 0.46 mm thick agarose and chicken breast tissue sections, respectively, using plane wave illumination. (c) Reconstruction of USAF target image through 0.46 mm thick chicken breast tissue using the OPC light field. The high quality of the reconstructed image attests that OPC light field can indeed suppress turbidity by retracing its initial trajectory through the tissue. RL: relay lens; L: imaging lens; CP: compensation plate; CCD: charged coupled device. Note that in all cases, the images are brought to the sharpest possible focus.

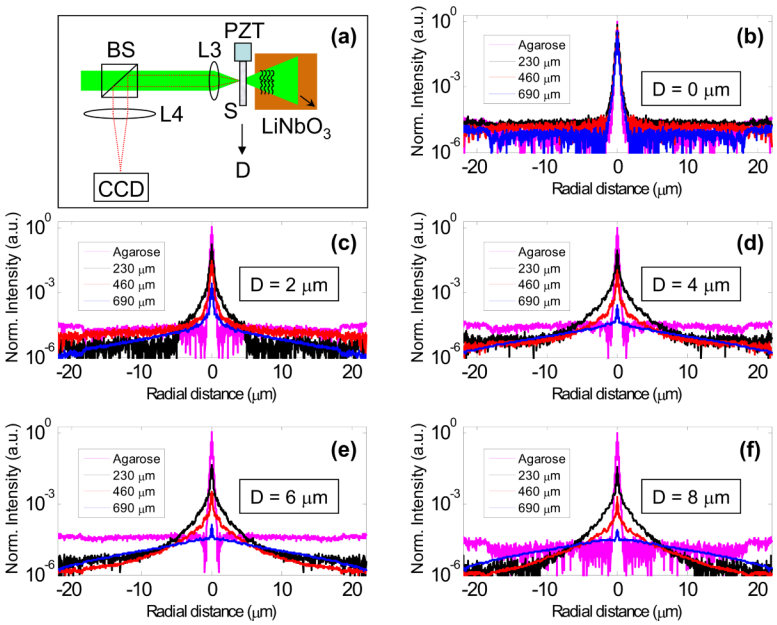

Figure 3. TSOPC using point source illumination

(a) Schematic of TSOPC experimental setup. (b)-(f) Average radial light intensity distributions of the reconstructed spots for 0.23 mm agarose and 0.23 mm, 0.46 mm, and 0.69 mm thick chicken breast tissue sections at 0μm, 2μm, 4μm, 6μm, and 8μm displacements, respectively. PZT: lead zirconate titanate actuator; S: Sample; D: displacement of the agarose and chicken breast tissue samples; BS: beam splitter; Li: ith imaging lens.

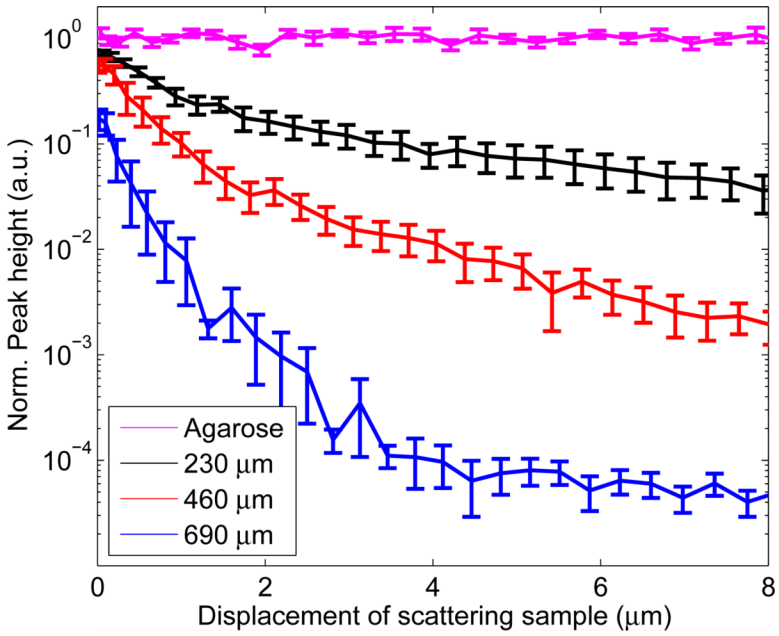

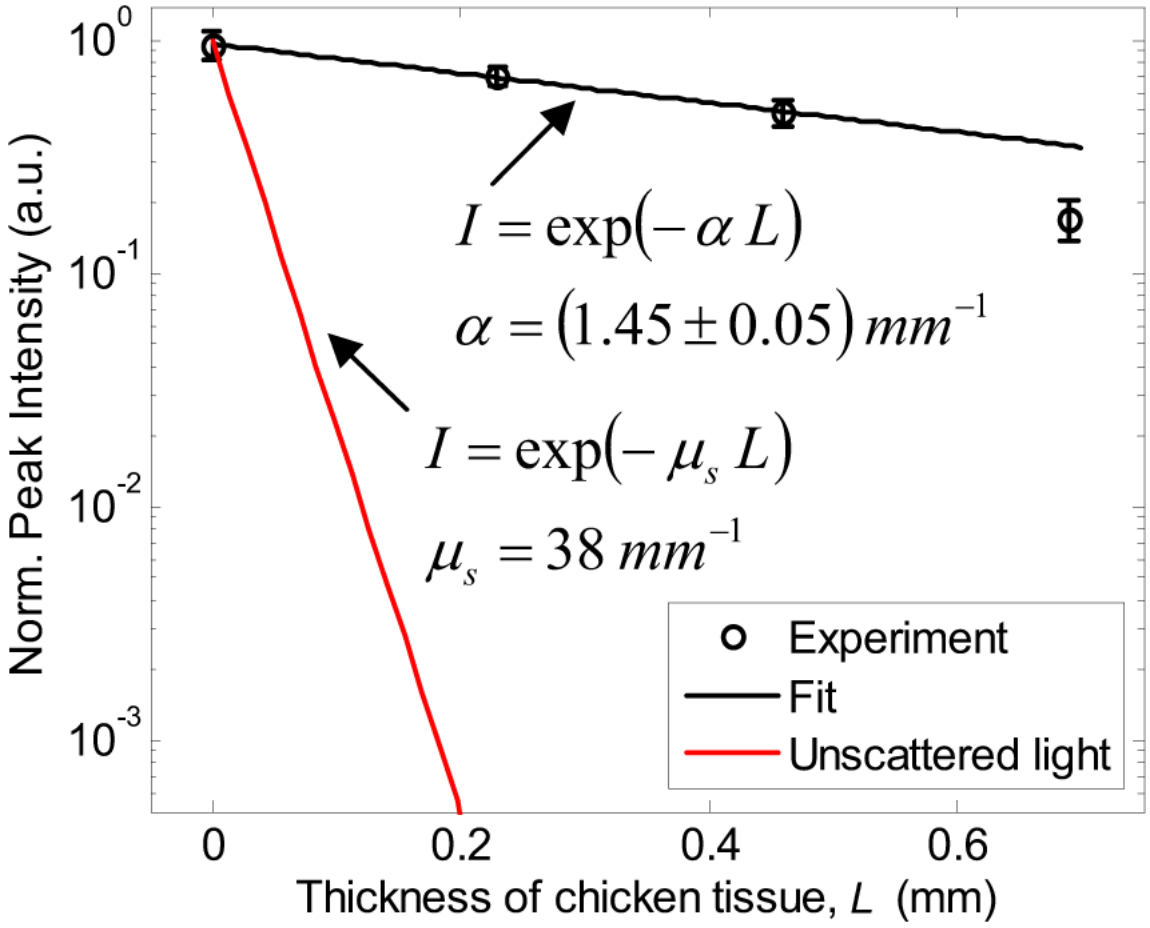

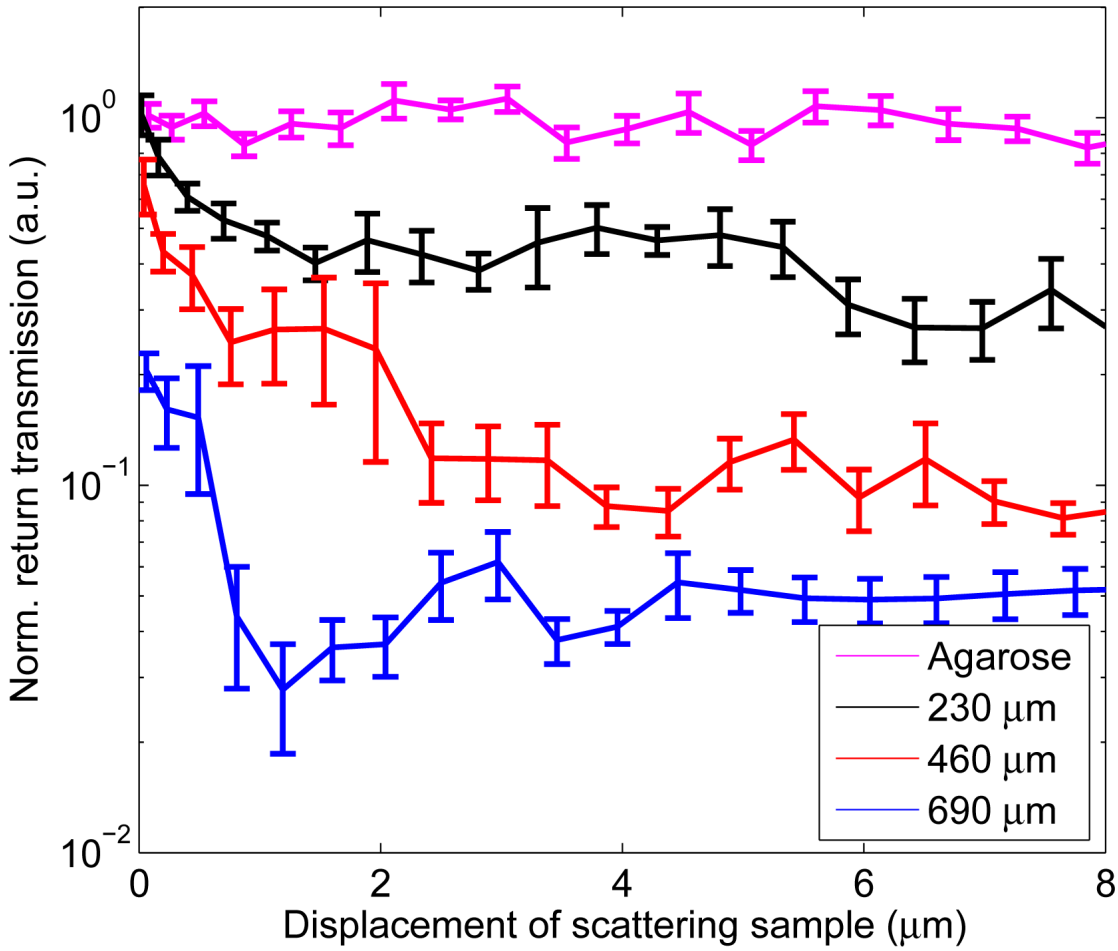

Figure 4. Strength of the reconstructed light field under OPC and non-OPC conditions

(a) Normalized peak intensity of the reconstructed spot versus (a) the displacement of chicken breast tissue sections of varied thicknesses and (b) the thickness of the chicken breast tissue sections for zero displacement. In Fig. 4(b), *I* is the normalized peak intensity of the reconstructed spot whereas α is the coefficient associated with the reconstruction efficiency drop. For comparison, the red line shows expected signal drop associated with coherence based detection methods. (c) Normalized return transmission reaching the CCD, within a collection angle of 29° from the PCM, versus the displacement of chicken breast tissue sections of different thicknesses. The error bar in each curve represents the standard error of the mean.

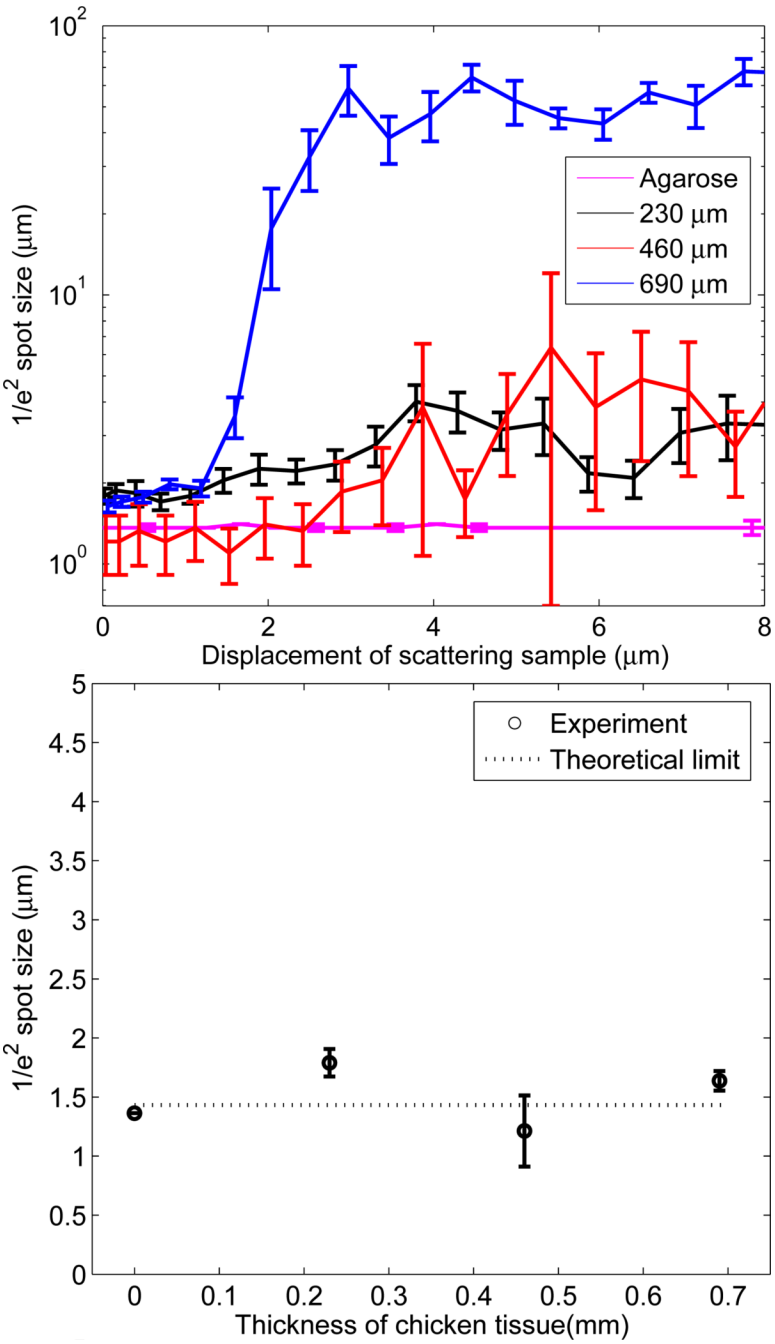

Figure 5. Quality of the reconstructed light field under OPC and non-OPC conditions

$1/e^2$ size of the reconstructed spot versus (a) the displacement of chicken tissue sections of different thicknesses and (b) the thickness of the chicken tissue sections for zero displacement. This illustrates that the reconstructed spot size for the ideal case (no sample displacement) is independent of the tissue thickness for tissues of up to 0.69 mm in thickness. The error bar in each curve represents the standard error of the mean.